Arctic sea ice parameters from AMSR-E data using two techniques and comparisons with sea ice from SSM/I

Josefino C. Comiso[1] and Claire L. Parkinson[1]

Received 30 March 2007; revised 13 September 2007; accepted 13 December 2007; published 21 February 2008.

[1] We use two algorithms to process Advanced Microwave Scanning Radiometer for the Earth Observing System (AMSR-E) data in order to determine algorithm dependence, if any, on the estimates of sea ice concentration, ice extent and area, and trends and to evaluate how AMSR-E data compare with historical Special Sensor Microwave Imager (SSM/I) data. The monthly ice concentrations derived from the two algorithms from AMSR-E data (the AMSR-E bootstrap algorithm, or ABA, and the enhanced NASA team algorithm, or NT2), differ on average by about 1–3%, with data from the consolidated ice region being comparable for ABA and NT2 retrievals while data in the marginal ice zones and thin ice regions show slightly higher values when the NT2 algorithm is used. The ice extents and areas derived separately from AMSR-E using these two algorithms are, however, in good agreement, with the differences (ABA – NT2) being about 0.07×10^6 km^2 on average for ice extents and -0.07×10^6 km^2 for ice area, which are small compared with mean seasonal values of 10.5×10^6 and 9.8×10^6 for ice extent and area, respectively. Likewise, extents and areas derived from the same algorithm but from AMSR-E and SSM/I data are consistent but differ by about 0.24×10^6 km^2 and 0.14×10^6 km^2, respectively. The discrepancies are larger with the estimates of extents than area mainly because of differences in channel selection and sensor resolutions. Trends in extent during the AMSR-E era were also estimated, and results from all three data sets are shown to be in good agreement (within errors).

Citation: Comiso, J. C., and C. L. Parkinson (2008), Arctic sea ice parameters from AMSR-E data using two techniques and comparisons with sea ice from SSM/I, *J. Geophys. Res.*, *113*, C02S05, doi:10.1029/2007JC004255.

1. Introduction

[2] The extent and area of the sea ice cover are key parameters needed to assess the state of the cryosphere and monitor the Earth's climate system. Prior to satellites, knowledge about these parameters was scant and inferred from limited human observations in different parts of the Arctic [*Walsh and Johnson*, 1979]. With the pan-Arctic ice cover so vast and dynamic, it was not until the advent of satellite remote sensing that quantitative assessments of the extent and area of sea ice for the entire Northern Hemisphere could be made. Among the first such estimates were those derived from data provided by the Electrically Scanning Microwave Radiometer (ESMR), which is a single channel system (at 19 GHz) launched in December 1972 aboard NASA's Nimbus 5 satellite [*Parkinson et al.*, 1987]. These data were suitable for estimates of the extent of sea ice covered areas because of the large contrast in emissivity between sea ice and liquid water. However, there were ambiguities in the estimates of sea ice concentration primarily because of large differences in the emissivity of seasonal first year (FY) ice and multiyear (MY) ice [*Vant et al.*, 1974; *Comiso*, 1983] and the difficulty of discriminating the latter from mixtures of open water and first year ice. The launch of the Scanning Multichannel Microwave Radiometer (SMMR) on board NASA's Nimbus 7 satellite in October 1978 made it possible to overcome the problem because of its multifrequency and multipolarization capability, which enabled the accounting of spatial changes in the emissivity of the surface. SMMR was followed by a similar instrument called the Special Sensor Microwave Imager (SSM/I), first launched in June 1987 on the F8 satellite in the Defense Meteorological Satellite Program (DMSP) series. Additional SSM/I instruments have been launched on the F11 and F13 satellites. The SSM/I sensors are considered "operational" rather than "research" instruments and are launched in succession to ensure that as one degrades or fails to operate, it is replaced by another. The combination of the SMMR and SSM/I instruments has enabled a near-continuous time series of consistent data on sea ice to be generated from November 1978 to the present.

[3] A new satellite microwave sensor from Japan called the Advanced Microwave Scanning Radiometer for the Earth Observing System (AMSR-E) was launched on board NASA's Aqua satellite in May 2002 with capabilities that exceed those of SMMR and SSM/I because of a larger

[1]Cryospheric Sciences Branch, NASA Goddard Space Flight Center, Greenbelt, Maryland, USA.

This paper is not subject to U.S. copyright.
Published in 2008 by the American Geophysical Union.

antenna (yielding higher spatial resolution) and wider spectral range. The new AMSR-E data indeed provide superior coverage of the sea ice cover and will likely be the baseline for studies of the ice cover in the years to come [*Comiso et al.*, 2003; *Markus and Cavalieri*, 2000]. However, its capabilities need to be evaluated and validated and also should be compared quantitatively with those of SSM/I and SMMR data. The ice concentrations from AMSR-E have been shown to be consistent with those from Aqua's Moderate Resolution Imaging Spectroradiometer (MODIS), which provides concurrent high-resolution visible and infrared data, and also with Landsat data [*Comiso*, 2004]. The goal is to be able to assess the accuracy of data that are currently used for monitoring the changes in the sea ice cover. While rapid declines have been reported in the Arctic perennial ice cover [*Comiso*, 2002; *Comiso and Parkinson*, 2004] the trends for the entire Northern Hemisphere have been more modest at about 3% per decade [e.g., *Bjorgo et al.*, 1997; *Cavalieri et al.*, 1997; *Parkinson et al.*, 1999]. Accurate data are also needed to validate modeling studies that have projected declines in the ice cover due to global warming caused in part by increasing greenhouse gases in the atmosphere [*Holland and Bitz*, 2003]. In this study, we assess the general characteristics of the Arctic sea ice cover as inferred from two sea ice algorithms. In particular we compare sea ice concentrations derived from these algorithms and assess quantitatively how the differences are reflected in estimates of sea ice extents, ice areas and trends. This enables us to examine whether the characterization of the sea ice cover is algorithm-dependent and if so, why. Also, we compare AMSR-E data with SSM/I data, to assess how the new data set can be used in conjunction with historical data to improve our characterization of the state of the sea ice cover. A companion paper [*Parkinson and Comiso*, 2008] examines the Antarctic sea ice cover with the same two algorithms and instruments.

2. Ice Algorithms, Data Reduction, Masks, and Sensitivity Studies

[4] The AMSR-E sensor has a total of 14 channels and measures microwave radiation from the Earth's surface at 7 frequencies (from 6.9 to 89.0 GHz) and at both vertical and horizontal polarizations. It is a conically scanning system with a swath width of about 1445 km and obtains data from practically the entire Arctic in less than a day, with an incidence angle fixed at about 55°. The instantaneous field of view of the sensor is 74 by 43 km at 6.9 GHz, improving with frequency to about 6 by 4 km at 89.0 GHz. The key AMSR-E frequencies that have been used for sea ice algorithms are 18.7 GHz and 36.5 GHz, with estimated ground resolution of about 27 by 16 km and 14 by 8 km, respectively. For comparison, the corresponding ground resolutions for the SMMR and SSM/I data at approximately the same frequencies are 54 by 35 km and 28 by 18 km for SMMR and 70 by 40 km and 38 by 30 km for SSM/I. The improvement in the resolution of AMSR-E data over those of historical data is therefore quite considerable. The resolution of AMSR-E at 89 GHz as indicated above is even better and could be utilized for many mesoscale studies; the 89 GHz resolution approaches that of the Advanced Very High Resolution Radiometer (AVHRR) Global Area Coverage (GAC) data, which have been used for detecting leads within the ice pack during cloud free conditions. However, the discrepancy of AMSR-E resolution with those of historical data requires special attention in order to obtain sea ice results consistent with the historical record. The 89 GHz data are promising in view of their spatial resolution but are difficult to use because of high sensitivity to atmospheric conditions and snow cover.

[5] Orbital AMSR-E data have been mapped to a polar stereographic grid at resolutions of about 12.5 by 12.5 km and 25 by 25.0 km using the "drop-in-a-bucket" technique, meaning that the near instantaneous brightness temperature observed by the sensor at a certain latitude and longitude point is assigned to an (i,j) grid element that encloses this geographical coordinate. To make the area of the polar grid nearly uniform, the mapping plane cuts the Earth's surface at 70° latitude. This gridding system has been used for generating daily averages of day and night data as well as daily sea ice data from AMSR-E and is consistent with the gridding system used with the SSM/I and SMMR sea ice data. The monthly maps used in this study are averages of daily data.

[6] Several sea ice concentration algorithms have been developed for multichannel passive microwave data over the years [e.g., *Cavalieri et al.*, 1984, *Swift et al.*, 1985; *Svendsen et al.*, 1987; *Comiso*, 1986; *Steffen et al.*, 1992]. The techniques have been refined and adapted for AMSR-E data, and for this study, we use two algorithms called the AMSR-E bootstrap algorithm (ABA) and the NASA team (version 2) algorithm (NT2), as discussed by *Comiso et al.* [2003].

[7] With a single channel, ice concentration (C) can be derived from satellite measurements of brightness temperature, T_B, using the following mixing equation that expresses the measurements as the sum of the two components of interest being sea ice (I) and open water (W):

$$T_B = C\,T_I + (1 - C)T_W \tag{1}$$

where T_I and T_W are the brightness temperatures or "tie points" of 100% ice and 100% open water (or 0% ice cover), respectively. Equation (1) looks simple, but the estimate of C is complicated by the large variability of the brightness temperature over ice covered and open water areas; hence the need for a more sophisticated algorithm, involving more than one channel. In the microwave region, following the Rayleigh-Jeans formulation, the brightness temperature can be estimated closely by the product of the emissivity and the temperature of the emitting surface. Although the emissivity of open water within the ice pack (which is usually under calm conditions) is reasonably stable, the emissivity of sea ice changes considerably depending on stage of ice growth, snow cover, thickness, and salinity. The physical temperature of the emitting layer, which is usually that of the snow/ice interface, is also variable although the changes are moderate (about 2.5°C standard deviation) after the sea ice has acquired a snow cover [*Comiso et al.*, 1989].

[8] The ABA technique identifies the tie points in equation (1) by making use of results from a cluster and regression analysis of sets of AMSR-E channels. The primary data sets used are those from 18.7 GHz at vertical

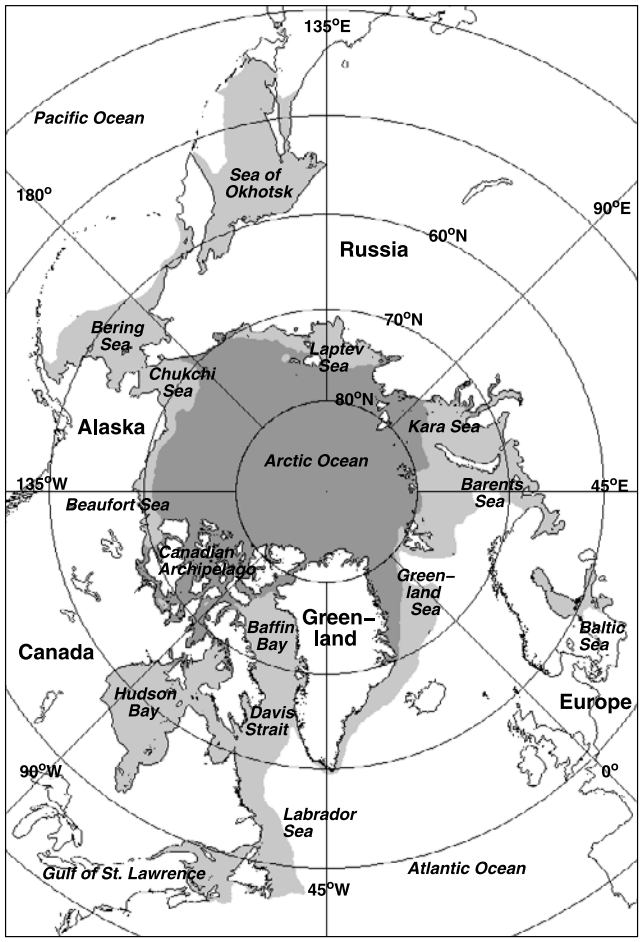

Figure 1. Location map of the Arctic, also showing sea ice distributions at the times of ice minimum and maximum, averaged for the years 1979–2006.

polarization and 36.5 GHz at both vertical and horizontal polarizations; these have reasonable resolution and predictable emissivities over ice covered areas, as discussed by *Comiso et al.* [2003]. The NT2 technique uses the same sets of channels formulated as gradient and polarization ratios, as in the original NT technique, and in addition makes use of the 89 GHz channel at vertical polarization to minimize errors associated with snow layering and other characteristics that affect one polarization channel more than the other [*Markus and Cavalieri*, 2000; *Comiso et al.*, 2003]. Because of the high sensitivity of the 89 GHz channel to snow and atmospheric effects, an atmospheric radiative transfer calculation is used to account for atmospheric influences in the radiative signal that reaches the satellite sensor. A challenge for the latter is how effectively a radiative transfer calculation can keep track of the surface emissivity at this frequency, which is unpredictably variable over sea ice covered regions. Previous comparative analysis of ice concentrations using the bootstrap and the NASA team algorithms showed large discrepancies [*Comiso et al.*, 1997]. The current study shows that the ice concentrations from the ABA and NT2 algorithms still have some discrepancies, but these are much smaller than those identified from the earlier versions of the algorithms [see *Comiso et al.*, 1997].

[9] A key concern with the use of data from different frequencies is the markedly different resolutions for the different frequency channels. The footprint of the 18.7, 36.5 and 89 GHz channels are 432, 112, and 24 km^2, respectively. Thus the instantaneous information that the AMSR-E 18.7 GHz sensor provides comes from an area about 18 times larger than that from the 89 GHz channel. The compromise solution is to use a grid resolution intermediate to the resolutions of 18.7 and 89 GHz and basically to degrade the resolution of the 89 GHz data. Two grid sizes are currently being used for mapping the AMSR-E sea ice data: 12.5 by 12.5 km (156.2 km^2) and 25 by 25 km (625 km^2). The use of the 12.5 by 12.5 km grid is justified in part by the fact that the distance between successive swaths along the satellite orbit is 10 km. Experience has shown that we get almost identical results from the 12.5 km gridded data and the 25 km data when the former is degraded to the resolution of the latter. For studies that require optimum resolution, the 89 GHz TB data have been mapped to a 6.25 by 6.25 km grid and ice concentration is derived using just the 89 GHz channels, e.g., using the bootstrap technique adjusted for the 89 GHz channels. Again, such data should be used with caution, in view of the sensitivity to atmospheric conditions and snow cover.

[10] Another source of concern is the information content of derived data from the different frequencies and polarization. For example, the contrast in emissivity between water and first year ice is higher with lower-frequency data. Also, the penetration depth through the snow and ice is frequency-dependent, with the radiation at lower frequencies (i.e., longer wavelengths) penetrating much deeper than the radiation at higher frequencies. Thus the radiation detected by the radiometers at different frequencies comes from different layers of the ice cover and, in some cases, even different types of layers. For example, the observed brightness temperature at 18.7 GHz from the seasonal ice cover usually originates from the snow/ice interface since snow is relatively transparent to radiation at this frequency, whereas at 89 GHz, the brightness temperature observed may come primarily from the snow cover. Also, the radiation at 18.7 GHz from multiyear ice originates from a thicker layer of ice and is therefore subject to volume scattering [*Eppler et al.*, 1992]. Therefore, although algorithms incorporating different channels are designed to produce the same ice concentration values, differences associated with the choice of channels can lead to somewhat different results. The discrepancies in the origin of the signals are in part taken into account through the use of scatterplots of sets of frequency (and polarization) channels that enable identification of signatures (i.e., tie points) of consolidated sea ice from the different frequency and polarization measurements. The choice of tie points is technique-dependent [*Comiso et al.*, 2003]; and a change in tie points results in different estimates for ice concentrations. The latter allows tie points to be used as "tuning" parameters for the ice concentration algorithms.

[11] An important consideration is that the multichannel signatures of different surfaces on land can be quite similar to those over sea ice. For simplicity, a land mask derived using published land boundaries and high-resolution satellite data, is used. Figure 1 provides a location map of land areas including small islands in the high-latitude regions of

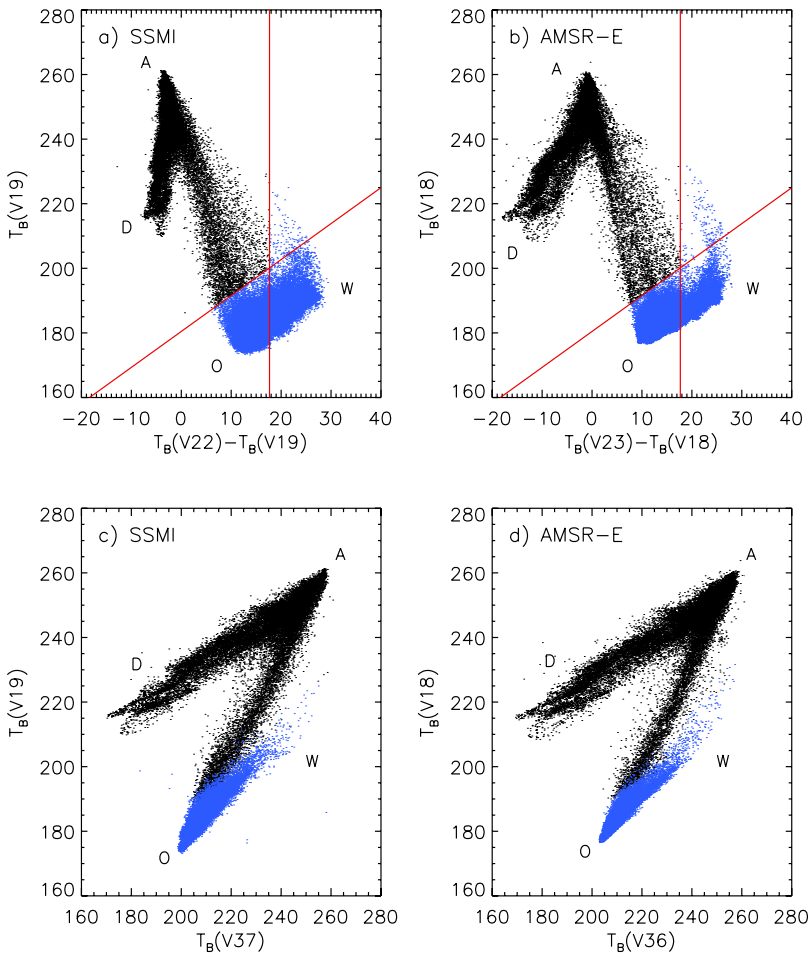

Figure 2. Scatterplots of brightness temperatures illustrating the distribution of open ocean area and the masking procedure using 19 GHz vertically polarized data (V19) versus the difference between 22 or 23 GHZ vertically polarized data (V22 or V23, respectively) and 19 or 18 GHz vertically polarized data (V19 or V18, respectively) from (a) SSM/I and (b) AMSR-E and V19 or V18 data versus 37 or 36 GHz vertically polarized data (V37 or V36, respectively) from (c) SSM/I and (d) AMSR-E. The mask for SMMR is similar to that in Figures 2c and 2d but has greater separation because SMMR has an 18 GHz channel (which is less subject to weather effects) instead of 19 GHz.

the Northern Hemisphere. Figure 1 also shows typical sea ice distributions during annual maximum and minimum ice coverage, as derived from historical satellite data. In winter, sea ice covers practically the entire Arctic basin and extends well out into many of the surrounding seas and bays. We know that the continental boundaries (generally delineated as extending to the edge of ice shelves where they exist) are actually not constant with time, especially in areas covered by ice shelves and glaciers, which are constantly changing because of melt, ice calving and surging. Unfortunately, a monitoring technique that keeps track of all continental boundary changes on a day-to-day basis currently does not exist, hence hindering the production of a land mask appropriate for each day (or even just each month) of data. With the observation of large calving events in recent years, such capabilities would be desirable. However, in this study, a fixed land mask is used for all data processed, with the same, constant land mask used for the ABA and NT2 algorithms. A notable advantage of the constant land mask is that it facilitates comparisons and determination of trends.

[12] A complication recognized since ice concentrations were first calculated from satellite data in the 1970s is that ocean data adjacent to the land-ocean boundaries are contaminated by signals from land. At these boundaries, there are data elements (pixels) that contain mixtures of land and ocean areas. In addition, radiometer sidelobe effects make the measurements at the ice edge different when the satellite crosses the boundary from land to ocean as opposed to ocean to land. Also, having footprints for some channels that are larger than the size of the grid causes a smearing effect. As a result, the algorithms yield nonzero ice concentrations near the land-ocean boundary (a few pixels beyond the boundary) even in regions that are unquestionably ice free, like along the coast of Spain. These faulty indications of ice would cause large errors in the estimates of ice extent and ice area if not corrected. To overcome this problem, the NT2 algorithm uses monthly sea surface temperature fields to establish a threshold for where sea ice is not allowed, and the bootstrap algorithm uses an enhanced version of a technique described by *Cho et al.*

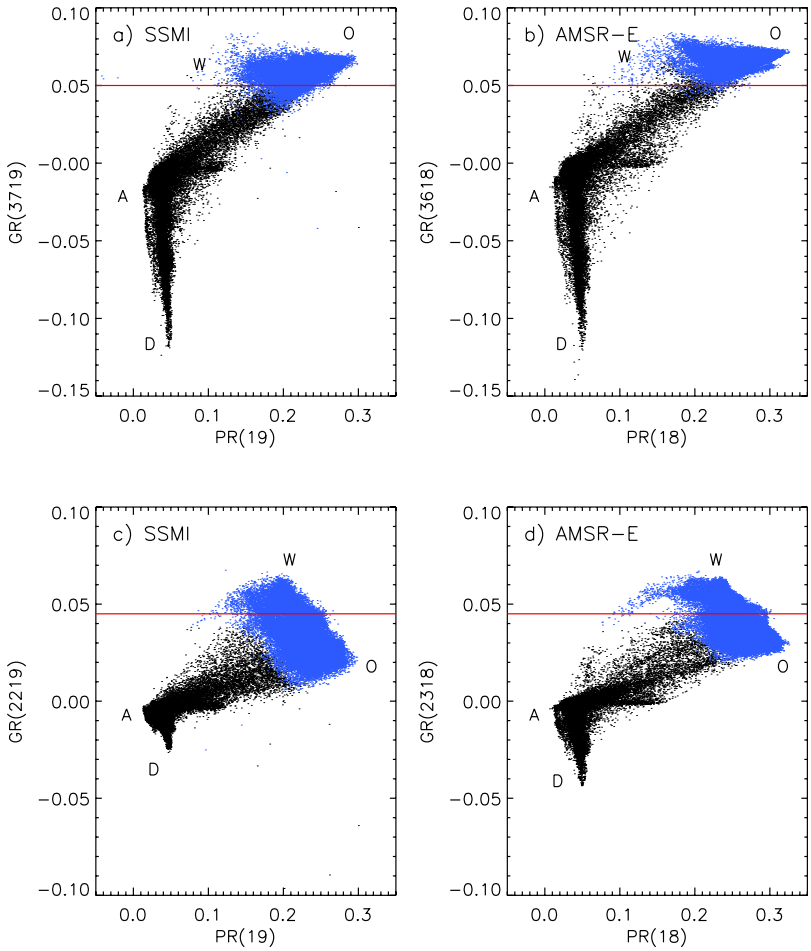

Figure 3. Scatterplots of gradient and polarization ratios illustrating the distribution of open ocean area using gradient ratio of V19 and V37 (GR3719) versus polarization ratio of H19 and V19 from (a) SSM/I and (b) AMSR-E data and also gradient ratio of V19 and V22 (GR2219) versus polarization ratio of H19 and V19 from (c) SSM/I and (d) AMSR-E data.

[1996], with residual derived ice cover that is clearly extraneous being removed manually or through temperature thresholds. Neither technique is perfect, but both considerably reduce the land contamination and weather effects.

[13] Extraneous nonzero ice concentrations at different but significant levels are also derived by the algorithms in the open ocean regions. This comes about because the microwave signatures of open ocean during adverse weather conditions with large waves, foam, and rain, can be similar to the signatures of ice covered ocean. For the bootstrap algorithm, a general filtering technique makes use of the unique patterns produced by data points belonging to ocean regions in scatterplots of different sets of AMSR-E channels as shown in Figure 2. Data from ice free ocean are represented in Figure 2 by the blue dots and can be classified as ice free areas by setting thresholds that separate them from ice covered areas. Ambiguities are not easy to eliminate since at the cutoff point near the ice edge, it is difficult to obtain a consistent threshold value in units of ice concentration because of the different emissivities of different sea ice types. Also, waves tend to cause ice rafting and flooding over the ice, both of which cause the ice emissivity to be even less well defined. The ocean masks employed by the bootstrap algorithm for SSM/I and AMSR-E data are illustrated in Figure 2, using the sets of 19, 22, and 37 GHz channels as shown. In the scatterplots in Figures 2a–2d, the data points that are clustered together between the labels O to W correspond to data in the open ocean. These data points (in blue) are easier to discriminate from the ice covered data points (in black) in Figures 2a and 2b, which make use of the 22 GHz channel (vertical polarization), than in Figures 2c and 2d. This is true generally, not just for the date illustrated in Figure 2, and hence the relationships reflected in Figures 2a and 2b are used as the primary mask for the SBA and ABA data set, while the relationships reflected in Figures 2c and 2d are used primarily to remove residuals. A slanted line which corresponds to ice concentrations of about 10% is drawn in the scatterplots and data below this line are considered ice free (or less than 10% ice concentration). Such a threshold is used since below 10% ice concentration, it is difficult to discriminate ice covered data from data without ice cover. In fact, in our ice concentration images we use a 12% threshold, and in our ice extent calculations we use a 15% threshold. The NT2 data set makes use of a similar masking technique but using gradient and polarization ratios in the scatterplot, as illustrated in Figures 3a and 3b for the

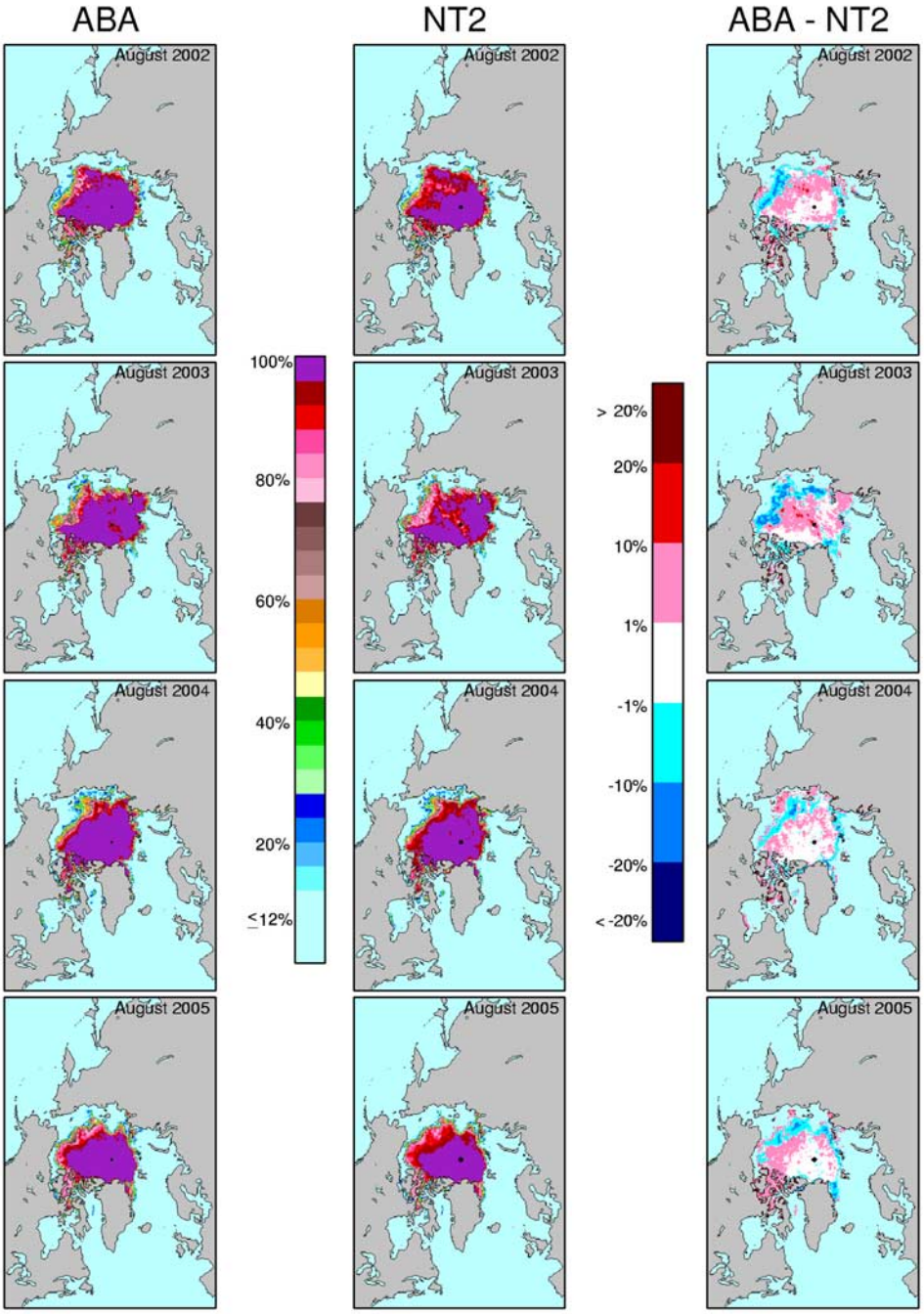

Figure 4. Color-coded monthly ice concentration maps derived from AMSR-E data for August 2002, 2003, 2004, and 2005 using the ABA and NT2 algorithms and the corresponding difference maps.

basic ocean mask for SSM/I and AMSR-E, respectively, supplemented by an additional mask using the gradient ratio between the 22 and 19 GHz channels, illustrated in Figures 3c and 3d, to remove residuals, as discussed by *Markus and Cavalieri* [2000].

[14] Some of the differences, especially in ice extent observed in this study, are associated with the differences in the data screened by the two techniques as either open water areas or ice covered areas. There are also differences in the "open ocean tie points" which are expected to represent the microwave signatures of open water within the ice pack. The clusters in Figure 2 and 3 provide the means to evaluate what this signature is; on the average, open water within the pack represents stable surface conditions that normally correspond to low brightness temperature values (i.e., close to the point O in Figures 2 and 3). Differences in tie point location affect the estimates of ice concentration, especially at low concentration values. To facilitate interpretation of the results when doing comparative analysis in this study, we make the masked areas in the open ocean and the land/ocean boundaries (especially in regions away from the ice pack) in the two data sets as consistent as possible.

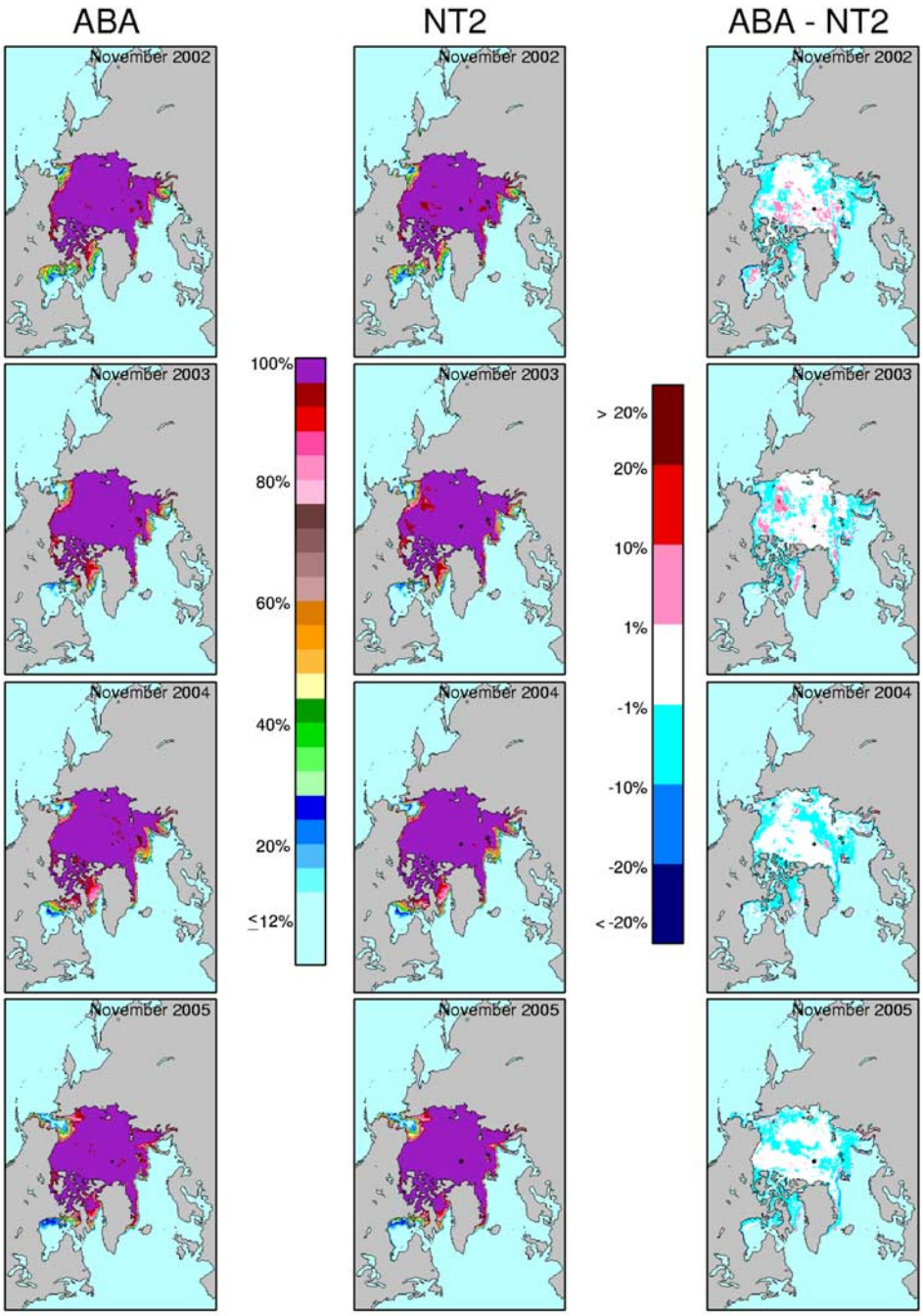

Figure 5. Same as Figure 4 but for November.

[15] The improvements of the AMSR-E versions of the bootstrap and NASA team algorithms over previous algorithms originally used for SSM/I and SMMR data are subtle but significant. The current capability of having high-resolution MODIS (250 m) data that are concurrent with AMSR-E data provided the means to optimize the tie points for each algorithm. The much higher resolution data from AMSR-E, especially at the 89 GHz channels, enabled the detection of mesoscale ice features like leads and polynyas and were also utilized for the same purpose. In the process, the original two-channel bootstrap algorithm that had been used for Antarctic sea ice was changed to the three-channel algorithm used in the Arctic, for improved accuracy and consistency in the retrieval. The NT2 algorithm was enhanced from the NT algorithm used for SSM/I data through the introduction of the 89 GHz channels to overcome problems that existed with polarization ratios at 37 GHz [*Comiso et al.*, 2003].

3. Ice Concentration Maps, Extents, and Ice Areas

3.1. Ice Concentrations

[16] Color-coded monthly ice concentration maps derived from AMSR-E data using the ABA and NT2 algorithms for

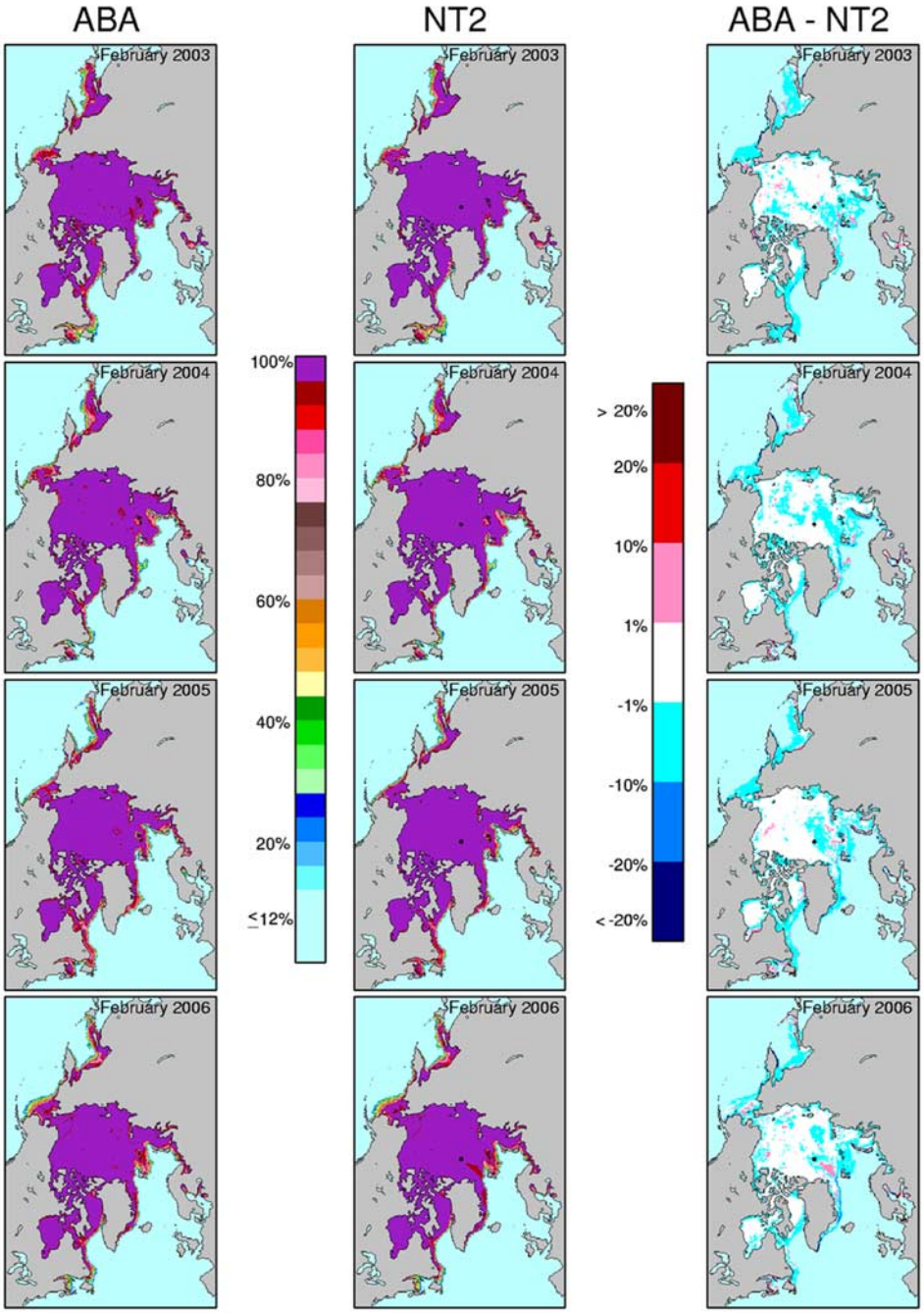

Figure 6. Same as Figure 4 but for February and for the years 2003–2006 rather than 2002–2005.

four different years in summer (August), autumn (November), winter (February), and spring (May) are presented in Figures 4, 5, 6, and 7, respectively, to illustrate the differences in ice concentrations calculated using the two different algorithms. Despite differences in the technique and sets of channels used, the monthly sea ice concentration maps from the two algorithms are fortunately quite similar, as both are attempting to depict the same parameter. In the sets of images, both algorithms yield very high concentrations within the ice pack, reflecting fully or near fully consolidated ice cover in the inner zone during the various periods, and good consistency in the location of the ice edges. There are subtle differences of usually less than 10% ice concentration and these are quantified better with the difference maps shown in the last column of Figures 3–6. In the inner pack, the ABA and NT2 concentrations are comparable, although with some areas of significant differences, while in the marginal ice zones, the ABA concentrations are usually less, especially in the nonsummer months.

[17] The differences in ice concentration are likely associated with use of different sets of channels in the two algorithms, as described in section 2. Perhaps most importantly, NT2 makes use of the 89 GHz channel in combination with the 19 and 37 GHz channels while ABA makes use of the 19 and 37 GHz channels only. The emissivity of sea ice generally increases with thickness up to a relatively stable

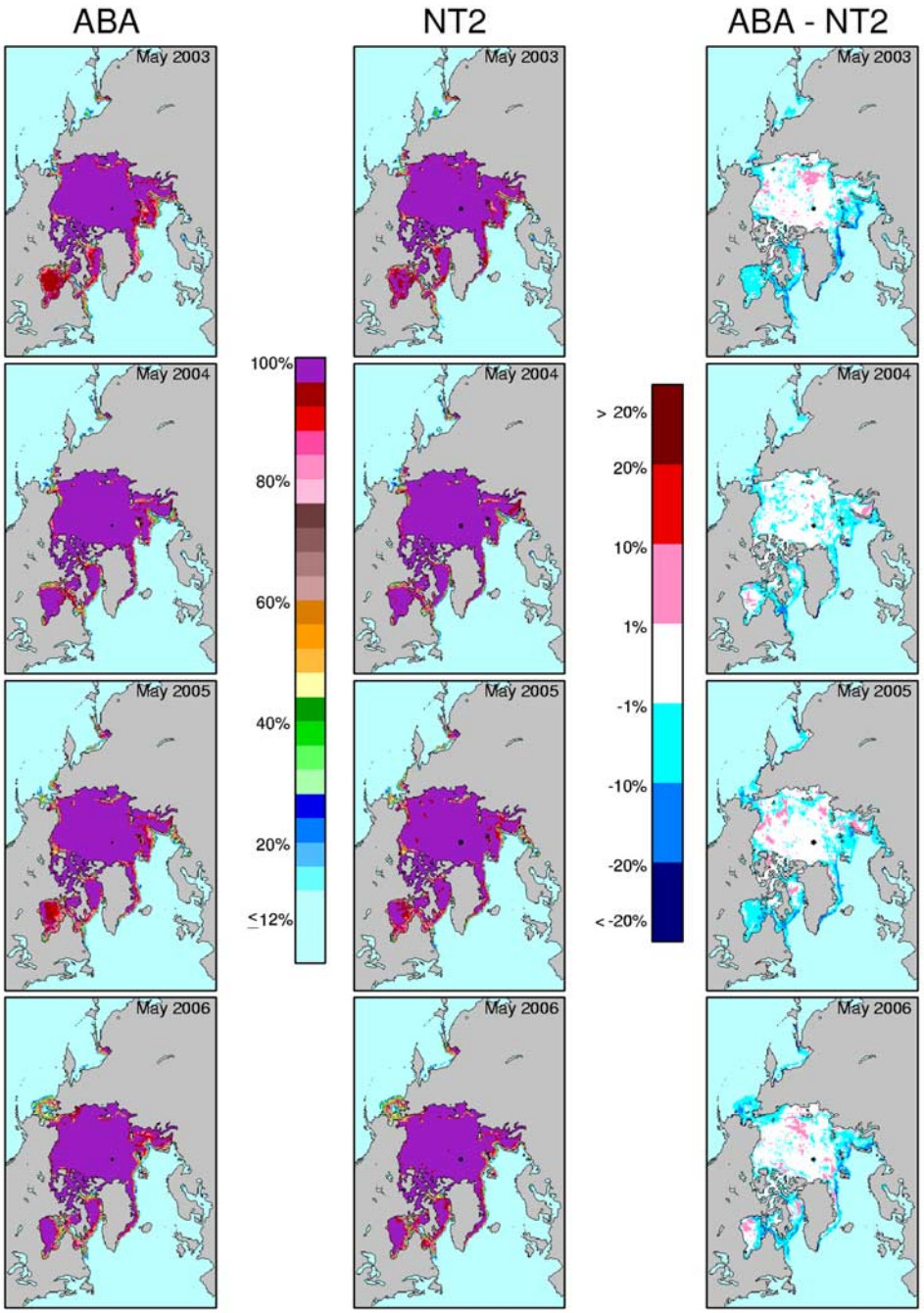

Figure 7. Same as Figure 6 but for May.

maximum value for first year (or seasonal) ice. This maximum value occurs at a certain thickness but the specific thickness varies with frequency (or wavelength of the radiation). This is because the penetration depth of the radiation varies inversely with frequency and therefore the maximum emissivity is reached when the ice is considerably thinner at 89 GHz than at 19 or 37 GHz. The use of a tie point that utilizes the 89 GHz data would therefore provide typically higher ice concentration values in the thin ice areas in the seasonal regions that those that use the lower frequencies only. However, the emissivity of ice at 89 GHz is not as stable over consolidated ice, and this may in part explain why the ice concentrations inside the pack in the Arctic basin are often higher for the ABA than for the NT2. Among the few exceptions is the area near the North Pole in the February 2004 images (i.e., negative values in the difference maps); this might have been an area of divergence at the time and hence might have had considerable thin ice. The emissivity for seasonal ice changes with thickness and granularity of the snow cover, but the multichannel algorithms take this into account, at least in part. The emissivity of ice may also be affected by changes in brine distribution and overall ice salinity during early stages of growth.

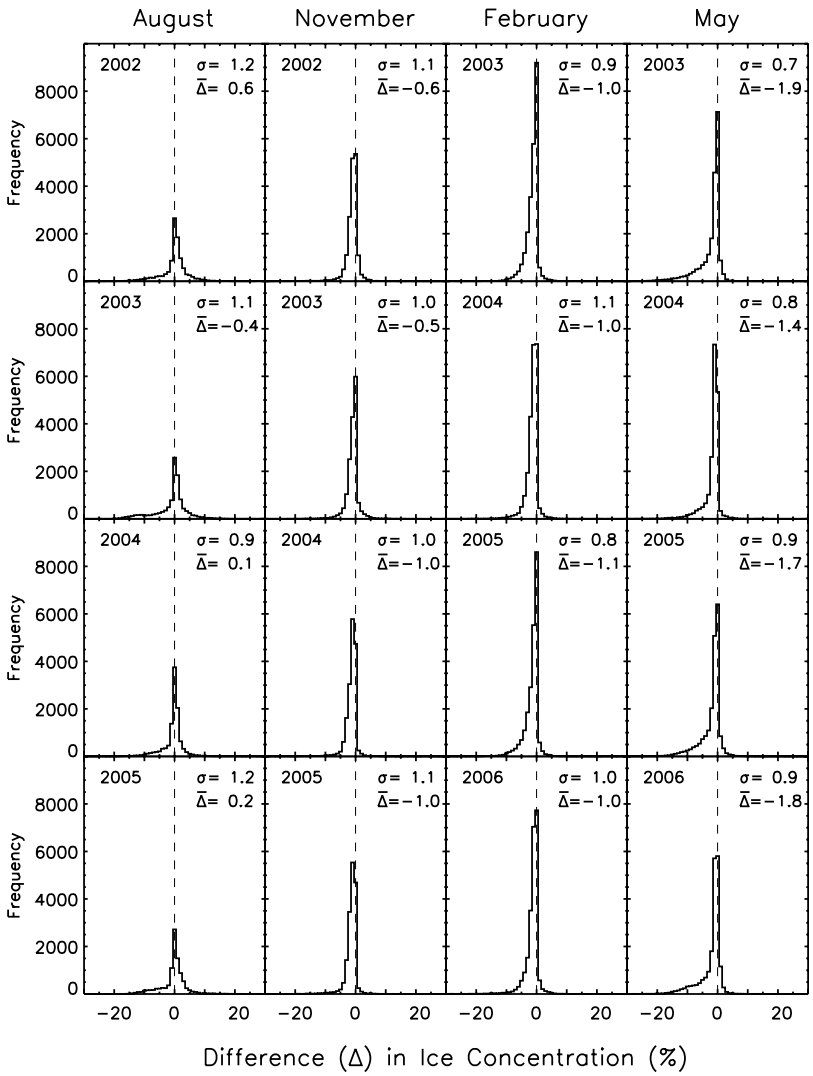

Figure 8. Histograms of differences in ice concentration (in percentage) between ABA and NT2. The standard deviation (σ) and the average of the ice concentration differences (Δ) for each plot are provided in the top right of each plot.

[18] During late spring and summer, the surface of the ice cover transforms first from a predominantly dry surface to a slightly wet surface and then to slush, with some areas covered by melt ponds (i.e., standing water on the surface of the ice floes). The emissivity of the surface during the early melt period is very high, almost similar to that of a blackbody, because at this stage, the presence of liquid makes the absorption coefficient of the snow very high. Further melt, however, transforms the material into slush, or almost melted snow, the emissivity of which is relatively low and close to that of water. As the snow continues to melt, the variability of the topography of the ice surface leads to the formation of melt ponds the signature of which is similar to that of open water [e.g., *Comiso and Kwok*, 1996; *Markus and Dokken*, 2002]. Thus the uncertainties in the estimates for ice concentration are greatest in summer, explaining in part why it is that the August images (Figure 4) are most different for the two algorithms. In the inner pack in August, data from the ABA overall show higher values, while near the ice edge, data from NT2 are generally higher. In autumn (Figure 5) the two sets of images are very similar but there are some areas of reduced ice concentrations in one but not in the other within the ice pack. Again, the marginal ice zones are locations of discrepancies. In the midwinter (Figure 6) the ice concentration maps are again very similar, with the difference maps showing mainly near-0 values in the inner pack and negative biases in the marginal ice zones. In spring (Figure 7), the distributions of ice cover as retrieved from the two algorithms are again in good agreement. It is interesting that in some seasonal areas like Hudson Bay, the differences were negative in 2003 and 2005 but primarily positive or near 0 in 2004 and 2006. This may be associated with the same melt phenomenon that occurs in summer.

[19] To assess the differences of the ABA and NT2 concentrations more quantitatively, histograms of the difference maps for the different years and seasons are presented in Figure 8. The histograms are highly peaked at a value near 0, indicating that the concentrations basically agree, although asymmetries are apparent, with a bias

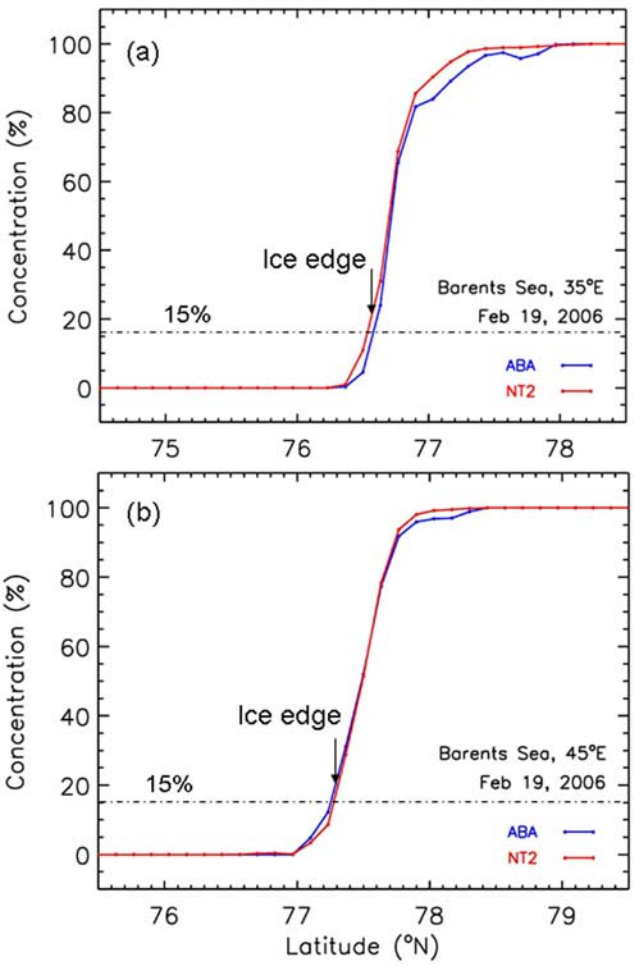

Figure 9. Ice concentration values along a transect from open water to the ice pack at (a) 35°E and (b) 45°E in the Barents Sea on 19 February 2006, as derived from AMSR-E data using the ABA and NT2 algorithms.

toward negative values in autumn, winter, and spring but toward positive values in summer, all in line with the images of Figures 4–7. The year-to-year variations for each of the four seasons are quite small. The peak value of the histograms varies with season, as expected, depicting the large seasonality of the sea ice cover. Gaussian fits were applied on each histogram, and the average standard deviation of the peaks (typically about ±1.0%) as well as the mean values of the differences are indicated in each plot.

3.2. Ice Extents and Areas

[20] To quantitatively assess the large-scale characteristics and state of the sea ice cover and its variability, we estimate the ice extents and ice area. Ice extent is the sum of the area of all data elements in the study region that have ice concentrations of 15% or higher. The 15% threshold is used because of aforementioned uncertainties in ice concentration values near the ice edges and thin ice regions and the possibility of including many faulty data points if the threshold is set at a lower level. This is also the threshold for ice extent used in many previous studies [e.g., *Parkinson et al.*, 1987, 1999]. Ice area is the integrated sum of the area covered by sea ice (i.e., sum of the products of the area of the pixel and the ice concentration in the pixel). In general, the ice extent provides the means to estimate the total area directly impacted by sea ice. On the other hand, the ice area provides actual ice coverage and the data needed in combination with average ice thickness to estimate total volume and mass of the ice cover. Both parameters are important in assessing how the state of the cryosphere as reflected by the sea ice cover is changing.

[21] Comparative analysis of ice concentration and extents requires considerations regarding how well the ice edges are represented by the different data sets. Plots of ice concentrations from a daily average map (specifically, one from 19 February 2006) along a transect from open water regions into the ice pack illustrates how the ice edges are represented by AMSR-E ice concentration data as derived from the ABA and NT2 algorithms (Figure 9). The plot is typical but with significant variations from one region to another. The data plotted are along longitudinal lines at 35°E and 45°E in the Barents Sea. At 35°E, the ice concentration data using ABA and NT2 both rise above 0% at approximately 76.4°N, with the NT2 data rising slightly more rapidly than the ABA data. Also, the ice concentrations for NT2 rise to near 100% in about 100 km and then remain near 100%, while the ABA ice concentrations remain below 100% for another 50 km, which suggests that the ABA is perhaps more sensitive to some features (e.g., thin ice) of the outer zone of the ice cover than the NT2. In this specific transect, the edge of the ice, as defined by 15% ice concentration in the calculation of ice extent, comes sooner (from open water into the pack) by about 5 km in the NT2 calculations than the ABA calculations. In much of the region near the ice edge, likely the ice cover consists mainly of pancake ice and is relatively mobile because of wind and wave action, the effect of which decreases, overall, from the ice edge into the pack. The latitude at which the ABA and NT2 ice concentration data both converge to about 100% is likely where the ice cover becomes consolidated and is no longer much affected by ocean swell. Similar phenomenon is apparent at 45°E, but this time the 15% ice edge occurs at about the same time and the values converge to 100% ice cover sooner into the pack. The space between pancakes is often covered by grease ice during autumn and winter; and the grease ice becomes the glue that transforms the region into consolidated ice. In contrast, the space between ice floes during spring and summer is often not covered by grease ice or other ice forms. As explained earlier, the average concentration in primarily new ice regions is expected to be higher with the NT2 than with the ABA, since the former saturates faster with thickness because of the use of the 89 GHz channel. In an area with considerable grease ice, NT2 likely captures the grease ice more accurately and obtains more accurate ice concentration values, while the ABA might provide more information regarding areas of divergence and the character of the marginal ice zone.

[22] Daily ice extent and area of the sea ice cover over an annual cycle (2005) in the Northern Hemisphere are presented in Figure 10 to illustrate how values derived from the NT2 and ABA algorithms differ. For comparison, in addition to the NT2 and ABA AMSR-E values, corresponding values from the SSM/I data using the bootstrap algorithm (SBA) are included in Figure 10 as well. The latter provide

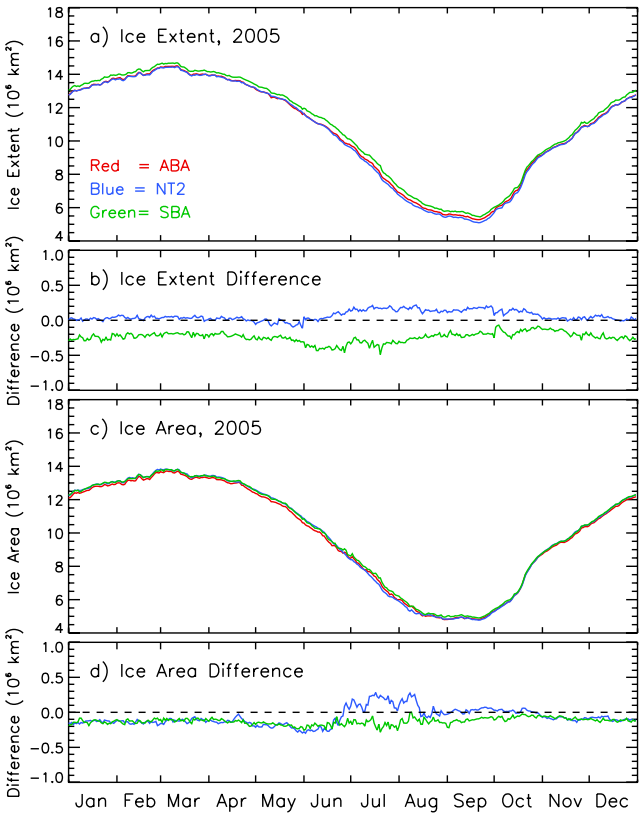

Figure 10. (a) Seasonal cycle of daily ice extent in 2005 using the ABA and NT2 algorithms on AMSR-E data and the SBA algorithm on SSM/I data, (b) difference in the ice extent seasonal cycle for ABA – NT2 (blue) and for ABA – SBA (green), (c) seasonal cycle of daily ice area in 2005 using the ABA and NT2 algorithms on AMSR-E data and the SBA algorithm on SSM/I data, and (d) difference in the ice area seasonal cycle for ABA – NT2 (blue) and for ABA – SBA (green).

the means to evaluate how data derived from different sensors but the same algorithm compare. Daily data are used to illustrate changes in these parameters at a smaller timescale than in the monthly averages. Although large daily changes are known to occur at the ice edge, the net changes in extent and area are modest in part because negative changes (or retreat) in one place are often compensated by positive changes (or advance) in other places. The plots indicate a reasonable consistency of extents and areas from the three data sets, although with the SBA data showing consistently higher values for extent than the other two. For more quantitative comparisons, differences between data sets are provided in Figures 10b and 10d. Monthly averages of the same parameters are also presented in Table 1. As explained earlier, higher values for extent can be caused by lower resolution, which is the case for SSM/I data. The differences in the ABA and NT2 extents are most pronounced during the summer, as reflected also in the ice concentration maps (Figures 4–7) while the areas are mainly consistent, especially during the autumn.

[23] Monthly averages of the ABA and NT2 ice extents and ice areas during the 2002–2006 period (when AMSR-E data are available) provide the means to assess monthly and interannual changes in the ice cover (Figures 11a and 11b). The variability in the extent and in the area are in part associated with the variability in the ice concentrations, the monthly averages of which are also shown in Figure 11c. The year-to-year variability in the ice extents during the AMSR-E era are consistently represented by ABA and NT2 data, with the summer season showing the largest difference (Figure 11), as in Figure 10. The ice areas have better consistency in the summer but show slight discrepancies in the winter period, with the NT2 values having slightly higher values. These wintertime discrepancies are reflected by the higher average ice concentrations derived from NT2 when compared with those from ABA mainly in the seasonal ice region (where mixtures of new ice and first year ice are more prevalent), as shown qualitatively in the color images in Figure 6 and quantitatively in the Figure 11c plots. Figure 11c shows that the mean ice concentrations from NT2 are consistently higher than those from ABA for all seasons except autumn, for which season some years (2002–2004) have practically the same mean ice concentrations from the two algorithms. However, throughout the time series the differences in the ice concentration values are less than 3%, which is within the published errors of the ice concentration algorithms [*Comiso et al.*, 2003]. Also, given the differences in the emissivity for the different ice types which vary in sensitivity to the different channels, such discrepancies in ice concentration are expected.

[24] Because of the relatively short record length, trend analyses of the AMSR-E data have limited use climatologically, but in this study we calculate trends in the ice cover in order to compare results from the two algorithms. Because of the large seasonality in the ice cover, trend analysis is done using anomalies calculated by subtracting from each data point (in our case, the monthly average for an individual year) the average for that specific month over each of the years of the record (in our case, 2002–2006). Plots of such anomalies for ice extent, ice area, and ice concentration, using both ABA and NT2 data, are presented in Figure 12, where it is apparent that the two data sets track each other very well, especially in ice extent and area. The trends in ice extent are −16.0 ± 1.8%/decade and −16.4 ± 1.8%/decade for the ABA and NT2 data, respectively, while the corresponding values for ice area are −16.1 ± 1.9%/decade and −15.9 ± 2.0%/decade. The good agreement indicates that despite some disagreements in the derived ice concentrations, the trends derived from the two sets of data are quite close.

[25] Figure 13 presents comparisons of AMSR-E and SSM/I monthly ice extents, ice areas, and ice concentrations, in this case using the bootstrap algorithm (ABA and SBA) to process data from two different sensors. The mean frequencies of the channels in the two sensors are slightly different, and therefore slight differences in sensitivity to atmospheric effects are expected. The main difference, however, is in the resolution, as indicated earlier, which is reflected in the higher values in extents derived from SSM/I data versus from AMSR-E data. The monthly ice areas are closer to each other, while the average ice concentrations are decidedly higher for the AMSR-E data than the SSM/I data. This implies that there are relatively more low ice concentration pixels in the SSM/I data than in the AMSR-E data. This affects the estimates of ice area less because the

Table 1. Comparison of ABA, NT2, and SBA Monthly Ice Extents and Areas in 2005

	ABA Ice Extent, $\times 10^6$ km^2	NT2 Ice Extent, $\times 10^6$ km^2	SBA Ice Extent, $\times 10^6$ km^2	ABA Ice Area, $\times 10^6$ km^2	NT2 Ice Area, $\times 10^6$ km^2	SBA Ice Area, $\times 10^6$ km^2
January	13.30	13.28	13.55	12.62	12.76	12.76
February	13.99	13.94	14.20	13.22	13.36	13.34
March	14.22	14.19	14.42	13.48	13.60	13.35
April	13.65	13.63	13.87	12.98	13.11	13.11
May	12.47	12.51	12.73	11.64	11.85	11.82
June	10.72	10.67	11.11	9.59	9.77	9.77
July	8.40	8.24	8.73	7.31	7.16	7.48
August	6.12	5.96	6.37	5.27	5.20	5.39
September	5.47	5.31	5.67	4.92	4.89	5.03
October	7.35	7.23	7.50	6.77	6.76	6.83
November	10.02	11.92	12.19	9.57	9.66	9.65
December	11.94	11.92	12.19	11.40	11.49	11.52

concentration is low and the net contribution to the ice area is therefore relatively minor.

[26] To evaluate how the trends compare when ice cover is derived from different sensors, the anomalies in ice extents and ice areas as well as ice concentrations are presented in Figure 14. The trends in ice extent calculated from the AMSR-E and SSM/I data sets with the bootstrap algorithm are shown to be fairly consistent, being −16.0 ± 1.8%/decade for AMSR-E and −15.8 ± 1.8%/decade for SSM/I. The corresponding trends in ice area are −16.1 ± 1.9 and 16.7 ± 1.9%/decade for AMSR-E and SSM/I, respectively. This is encouraging since it indicates that AMSR-E data can be combined with the other historical data to assess the trends of the sea ice cover if biases are taken into consideration.

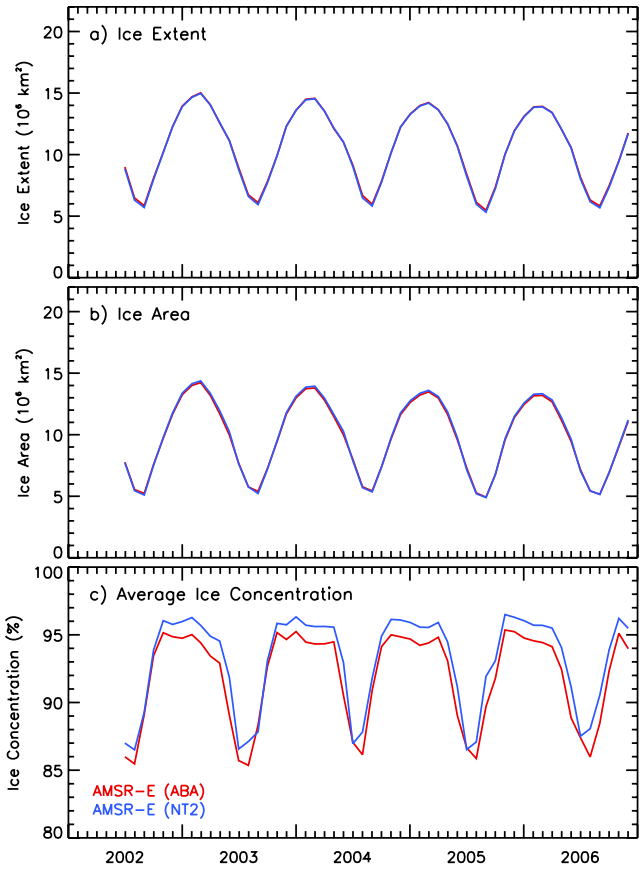

Figure 11. Plots of monthly values of (a) ice extent, (b) ice area, and (c) ice concentration from June 2002 through November 2006 derived from AMSR-E data using the ABA and NT2 algorithms. Each monthly ice concentration data point is the average of the daily ice concentration averages during the month.

4. Analysis of Errors

[27] In a few locations and times, there are significant differences in the ice concentrations derived from the AMSR-E data using the ABA and NT2 algorithms. The

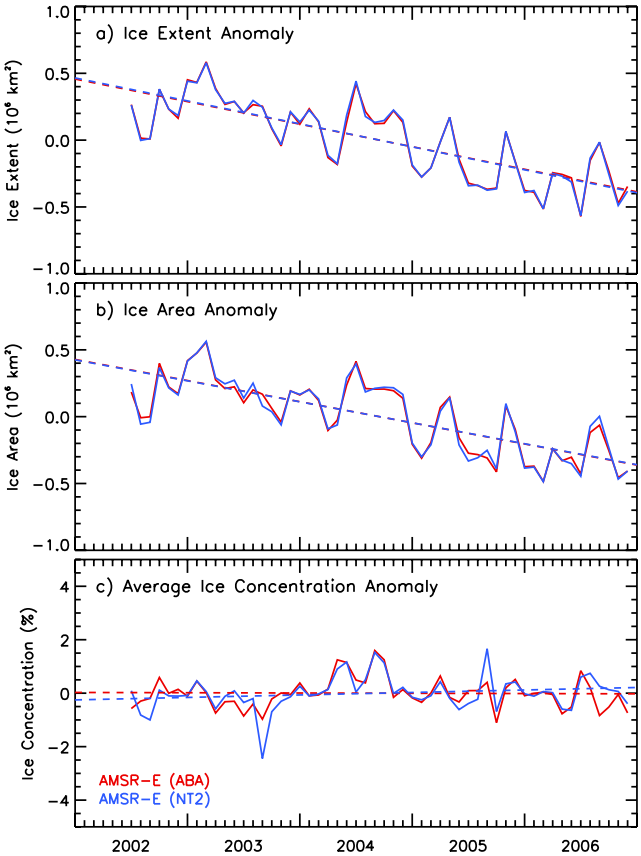

Figure 12. Plots of anomalies of the monthly values of (a) ice extent, (b) ice area, and (c) ice concentration from June 2002 through November 2006 derived from AMSR-E data using the ABA and NT2 algorithms.

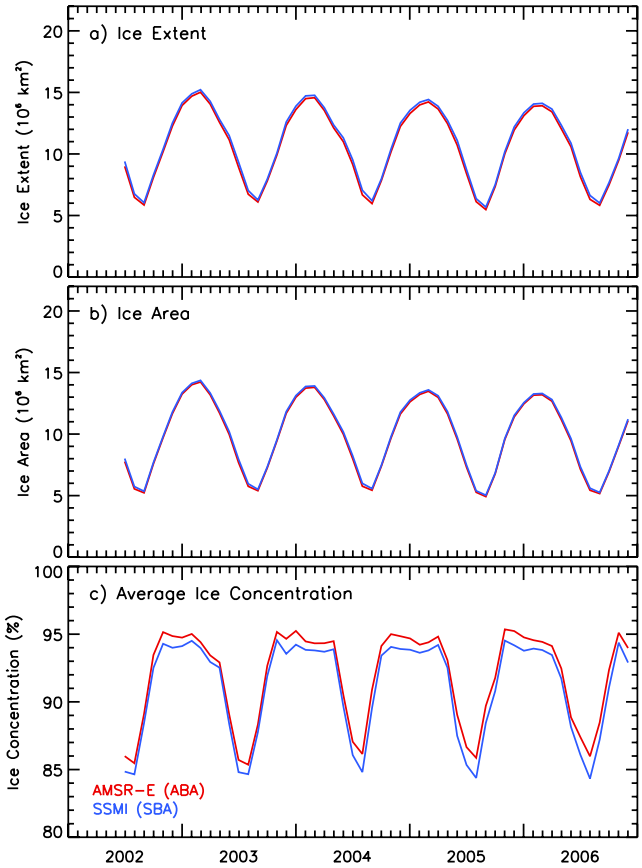

Figure 13. Plots of monthly values of (a) ice extent, (b) ice area, and (c) ice concentration from June 2002 through November 2006 derived from the AMSR-E and SSM/I data using the ABA algorithm. Each monthly ice concentration data point is the average of the daily ice concentration averages during the month.

difference maps in Figures 4–7 indicate that NT2 produces generally higher concentrations than ABA in the marginal ice zone regions in February, May, and November while in August, ABA values are higher than NT2 values in the perennial ice regions. The use of different sets of channels leads to differences in the characterization of ice edges and marginal ice zones, as illustrated in Figure 9, thereby causing differences in the estimates of ice extent. The choice of channels also leads to differences in the perennial ice regions since the emissivity of consolidated ice is spatially more variable with some channels (i.e., 89 GHz channels) than other channels. Nevertheless, there is reasonable agreement, with the differences typically being no more than about 3%, which is within the estimated errors of the ice concentration algorithms. The differences are minimized mainly because both algorithms make use of the same AMSR-E data to infer the tie points for consolidated ice and open water [*Comiso et al.*, 2003]. Slight adjustments in the tie points, although not trivial to select, could lead to a closer match in the ice concentration values, but not to identical values throughout, as there are features that one algorithm captures but the other algorithm does not. The cause of these subtle differences may be important to understand in special cases, such as studies of sensible and latent heat polynyas in which quantification of accurate estimates of heat, salinity, and humidity fluxes is desired [*Kwok et al.*, 2007].

[28] Errors in ice extent and area include those associated with the open ocean mask, land/ocean boundary mask, and land mask which are affected only indirectly by the sea ice concentration algorithms. In the Arctic, the uncertainties associated with these parameters can be large because of the presence of extensive ice-free coastlines and many islands, with the latter sometimes so small (compared with the standard grid size of 25 by 25 km) that they are not included as part of the landmass. The land mask is basically fixed, and using a fixed land mask has significant advantages for time series studies. However, as indicated earlier, coastline changes occur because of ice calving, erosion, and other phenomena. An associated question is whether to classify icebergs as part of the sea ice cover or not. The answer is likely no for mass balance studies but yes for many other applications. In the current analysis, icebergs are included in the ice cover calculations, because of failure to identify them properly and to separate them out. The icebergs are not included in full because the emissivity of icebergs is generally lower than that of thick seasonal ice, thereby producing a microwave signature of a partial sea ice cover.

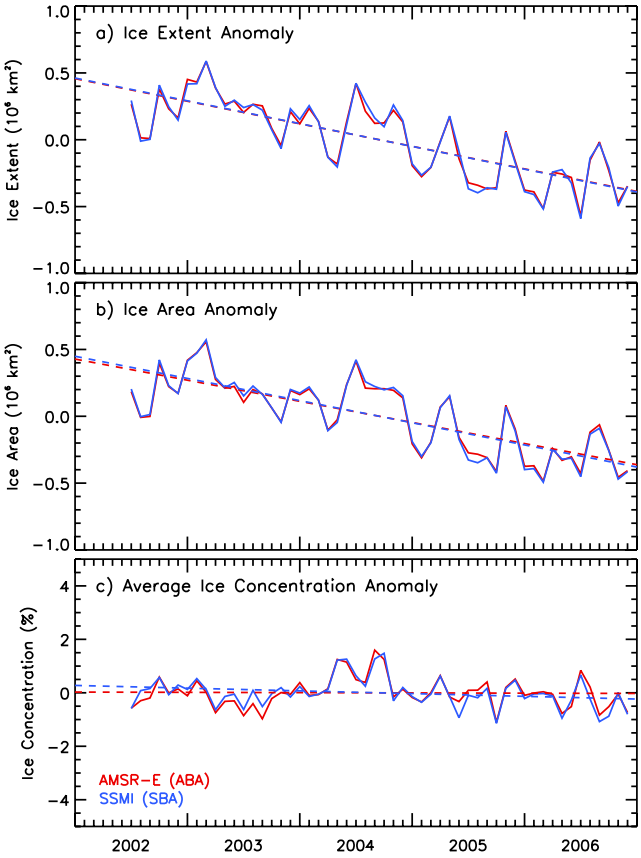

Figure 14. Plots of the anomalies of the monthly values of (a) ice extent, (b) ice area, and (c) ice concentration from June 2002 through November 2006 derived from the AMSR-E and SSM/I data using the bootstrap algorithm (ABA and SBA).

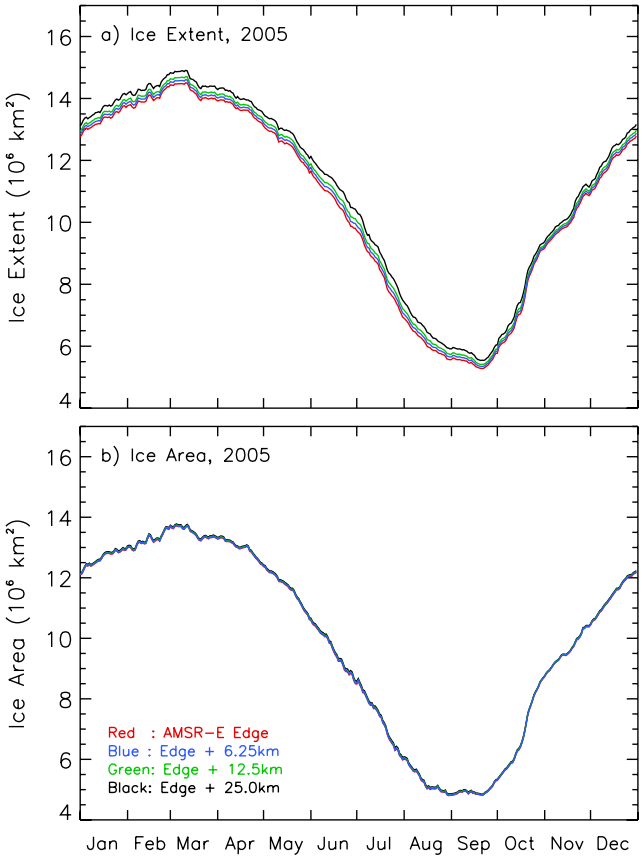

Figure 15. (a) Sensitivity plot of the seasonal cycle of monthly average ice extent, with the baseline curve being the AMSR-E extent and the additional curves being the extents derived if the ice edge is further south by 6.25, 12.5, and 25 km. (b) Sensitivity plot similar to Figure 15a but using monthly average ice area.

[29] As indicated earlier, the 15% ice edge as inferred from the two algorithms can vary by a few km. This is primarily because of the use of different channels with different resolutions but it can also be because of differences in the location of the tie point for open water. To get an assessment of errors in extent and area associated with errors in the location of the ice edge, we did sensitivity studies using actual data to examine how the ice extent and area change for an error in the ice edge of 6.25, 12.5 and 25 km. Given an ice distribution, we can either add or subtract this value along the ice edge and calculate the resulting change in extent; for the change in area, we assume that the added (or subtracted) data elements all have ice concentrations of 15%. Figure 15 shows the AMSR-E 2005 ice extent and area time series from the ABA algorithm, plus the result of extending the ice edge by 6.25, 12.5, and 25.0 km. Comparing ice extents as depicted in Figure 15 with Figure 10, one can infer that the difference between those of the NT2 and ABA can be explained by errors of about 6.25 km in the ice edge, except during the summer period when other factors must contribute to the difference. With ice area, the variability is similar during the summer but not in the other seasons, when other factors must contribute to the error.

[30] Errors associated with the use of SSM/I data can be evaluated in a similar manner. The biggest source of discrepancies in the SSM/I versus AMSR-E extents and areas is likely the resolution. The ice edge is better defined with AMSR-E data than with SSM/I data, with the SSM/I ice edges often about 12–25 km equatorward of the AMSR-E ice edge. Comparing the ice extents in Figures 15 and 10, the difference between the AMSR-E and SSM/I results can be explained by a 12.5 km ice edge error in the winter and autumn and a 25 km ice edge error in the spring and summer. With ice area, the difference is likely again caused primarily by other factors.

[31] It should also be pointed out that the ABA AMSR-E data that are currently being released by the National Snow and Ice Data Center (NSIDC) have been processed using a slightly different version of the algorithms for different time periods. Different versions are typically minor updates in the tie points to get better consistency with validation data. Because of the aforementioned changes from a two-channel to a three-channel algorithm for the Antarctic and some adjustments in the tie points for the Arctic, this study made used of ABA data that are derived consistently (with the same version) from 2002 to the present. Similar reprocessing has been planned for the NT2 but has not been implemented. However, only subtle changes in the derived data are expected in the NT2 time series as revealed by the lack of large year-to-year changes in the differences in our analysis.

[32] Special validation studies for the AMSR-E algorithms are currently in progress and preliminary analyses have shown promising results [*Cavalieri et al.*, 2006; *Massom et al.*, 2006; *Comiso*, 2004]. The implementation of a validation study in regions and in time periods where the two algorithms differ the most, however, is a complex endeavor and is not within the scope of this paper. Nevertheless, it is encouraging that overall, the differences between the two algorithms are within the errors that have been established using current validation data.

5. Discussion and Conclusions

[33] The Aqua AMSR-E sensor provides the opportunity to observe the Arctic sea ice cover at a higher resolution and greater spectral range than previously possible. The availability of the data is timely in light of rapid changes being observed in parts of the polar regions in recent years and the requirements of more accurate observations. We use ice concentrations derived from two AMSR-E algorithms to assess how consistently the ice cover can be characterized and how estimates of the Arctic sea ice extent and area as well as their trends would be affected by the use of different techniques. Such comparisons are especially important since the extent and area provide the means to assess the state of the sea ice cover and quantify impacts of Arctic warming that may be related to increasing anthropogenic greenhouse gases in the atmosphere. It is also essential to know to what extent such estimates can be algorithm-dependent.

[34] The monthly ice concentrations derived from AMSR-E data using the two algorithms differ on average by about 1–3%, with the derived ice concentrations from near the ice edge typically being higher when the NT2 algorithm is used. The standard deviations of the differences

are also very small, being ±1.1, ±1.0, ±0.9, and ±0.8% in summer, autumn, winter and spring, respectively. Slight adjustments in the tie points for ice and water could make the difference even smaller. It is encouraging to get very good consistency in the extents and areas of the sea ice cover as derived from AMSR-E data using two algorithms that are formulated quite differently and make use of different sets of AMSR-E channels, as it is highly desired that the characterization of the ice cover, including its ice extent and area, would be independent of technique, allowing for confidence in the results.

[35] Likewise, it is satisfying to get good agreement of extents and areas derived when data from AMSR-E are compared with those from SSM/I using the same algorithm. There are slight biases associated with the differences in the resolution of the different sensors in the estimates of ice extents but this is basically negligible in estimates of ice area. A bias, if uncorrected would cause significant errors when combining AMSR-E with historical data. Fortunately, a long overlap of AMSR-E and SSM/I data exists and this will provide the means to remove biases before incorporating the AMSR-E data in the time series.

[36] The discrepancies in the derived ice concentrations (and also extents and areas) from AMSR-E data using the ABA and NT2 algorithms are likely associated mainly with the choice of channels and in part the choice of tie points. Different channels have different sensitivities to different surfaces. This is especially the case in seasonal regions where new ice is abundant. The use of high-frequency channels like the 89 GHz channel, as with NT2, provides the means to identify thin ice; however, the channel is sensitive to atmospheric and surface effects and can produce erroneous ice concentrations if such sensitivity is not properly taken into account. The use of lower-frequency channels, as with ABA, provides more contrast between open water and sea ice covered regions and less sensitivity to atmospheric and surface effects but classifies thin ice as having relatively lower concentration than thick ice because of lower emissivity. While this reflects an error in ice concentration (if new ice and thick ice are treated as identical in an ice concentration algorithm), it allows improved ability to assess the widths of the marginal ice zones more accurately and allows the detection of divergence and polynya regions. Overall, the merit of each algorithm depends on application but it is encouraging to know that they produce approximately the same trends in ice extent and area and that the differences in ice concentration values are well within the 5–10% estimated errors in the ice concentration determinations.

[37] **Acknowledgments.** The authors gratefully appreciate the excellent programming support provided by Robert Gersten of Adnet/RSIS and Nick DiGirolamo of SSAI. The project was funded by the Cryospheric Sciences Program at NASA Headquarters.

References

Bjorgo, E., O. M. Johannessen, and M. W. Miles (1997), Analysis of merged SMMR-SSMI time series of Arctic and Antarctic sea ice parameters 1978–1995, *Geophys. Res. Lett.*, *24*(4), 413–416.

Cavalieri, D. J., P. Gloersen, and W. J. Campbell (1984), Determination of sea ice parameters with the Nimbus 7 SMMR, *J. Geophys. Res.*, *89*(D4), 5355–5369.

Cavalieri, D. J., P. Gloersen, C. Parkinson, J. Comiso, and H. J. Zwally (1997), Observed hemispheric asymmetry in global sea ice changes, *Science*, *278*(7), 1104–1106.

Cavalieri, D. J., T. Markus, D. K. Hall, A. J. Gasiewski, M. Klein, and A. Ivanoff (2006), Assessment of EOS Aqua AMSR-E Arctic sea ice concentrations using Landsat-7 and Airborne microwave imagery, *IEEE Trans. Geosci. Remote Sensing*, *44*(11), 3057–3069.

Cho, K., N. Sasaki, H. Shimoda, T. Sakata, and F. Nishio (1996), Evaluation and improvement of SSM/I sea ice concentration algorithms for the Sea of Okhotsk, *J. Remote Sens. Jpn.*, *16*(2), 47–58.

Comiso, J. C. (1983), Sea ice microwave emissivities from satellite passive microwave and infrared observations, *J. Geophys. Res.*, *88*(C12), 7686–7704.

Comiso, J. C. (1986), Characteristics of winter sea ice from satellite multispectral microwave observations, *J. Geophys. Rev.*, *91*(C1), 975–994.

Comiso, J. C. (2002), A rapidly declining perennial sea ice cover in the Arctic, *Geophys. Res. Lett.*, *29*(20), 1956, doi:10.1029/2002GL015650.

Comiso, J. C. (2004), Sea ice algorithm for AMSR-E, *It. J. Remote Sens.*, *30/31*, 119–130.

Comiso, J. C., and R. Kwok (1996), The summer Arctic sea ice cover from satellite observations, *J. Geophys. Res.*, *101*(C2), 28,397–28,416.

Comiso, J. C., and C. L. Parkinson (2004), Satellite observed changes in the Arctic, *Phys. Today*, *57*(8), 38–44.

Comiso, J. C., T. C. Grenfell, D. L. Bell, M. A. Lange, and S. F. Ackley (1989), Passive microwave in situ observations of winter Weddell sea ice, *J. Geophys. Res.*, *94*(C8), 10,891–10,905.

Comiso, J. C., D. J. Cavalieri, C. L. Parkinson, and P. Gloersen (1997), Passive microwave algorithms for sea ice concentration: A comparison of two techniques, *Remote Sens. Environ.*, *60*(3), 357–384.

Comiso, J. C., D. J. Cavalieri, and T. Markus (2003), Sea ice concentration, ice temperature, and snow depth using AMSR-E data, *IEEE Trans. Geosci. Remote Sens.*, *41*(2), 243–252.

Eppler, D., et al. (1992), Passive microwave signatures of sea ice, in *Microwave Remote Sensing of Sea Ice*, *Geophys. Monogr. Ser.*, vol. 68, edited by F. D. Carsey, pp. 47–71, AGU, Washington, D. C.

Holland, M. M., and C. M. Bitz (2003), Polar amplification of climate change in the Coupled Model Intercomparison Project, *Clim. Dyn.*, *21*, 221–232.

Kwok, R., J. C. Comiso, S. Martin, and R. Drucker (2007), Ross Sea polynyas: Response of ice concentration retrievals to large areas of thin ice, *J. Geophys. Res.*, *112*, C12012, doi:10.1029/2006JC003967.

Markus, T., and D. J. Cavalieri (2000), An enhancement of the NASA team sea ice algorithm, *IEEE Trans. Geosci. Remote Sens.*, *38*(3), 1387–1398.

Markus, T., and S. T. Dokken (2002), Evaluation of Arctic late summer passive microwave sea ice retrievals, *IEEE Trans. Geosci. Remote Sens.*, *40*, 348–356.

Massom, R. A., et al. (2006), ARISE (Antarctic Remote Ice Sensing Experiment) in the East 2003: Validation of satellite-derived sea-ice data products, *Ann. Glaciol.*, *44*, 288–296.

Parkinson, C. L., and J. C. Comiso (2008), Antarctic sea ice parameters from AMSR-E data using two techniques and comparisons with sea ice from SSM/I, *J. Geophys. Res.*, doi:10.1029/2007JC004253, in press.

Parkinson, C. L., J. C. Comiso, H. J. Zwally, D. J. Cavalieri, P. Gloersen, and W. J. Campbell (1987), Arctic sea ice, 1973–1976: Satellite passive-microwave observations, *NASA Spec. Publ.*, *489*, 296 pp.

Parkinson, C. L., D. J. Cavalieri, P. Gloersen, H. J. Zwally, and J. C. Comiso (1999), Arctic sea ice extents, areas, and trends, 1978–1996, *J. Geophys. Res.*, *104*(C9), 20,837–20,856.

Steffen, K., D. J. Cavalieri, J. C. Comiso, K. St. Germain, P. Gloersen, J. Key, and I. Rubinstein (1992), The estimation of geophysical parameters using passive microwave algorithms, in *Microwave Remote Sensing of Sea Ice*, *Geophys. Monogr. Ser.*, vol. 68, edited by F. D. Carsey, pp. 201–231, AGU, Washington, D. C.

Svendsen, E., C. Matzler, and T. C. Grenfell (1987), A model for retrieving total sea ice concentration from a spaceborne dual-polarized passive microwave instrument operating near 90 GHz, *Int. J. Remote Sens.*, *8*, 1479–1487.

Swift, C. T., L. S. Fedor, and R. O. Ramseier (1985), An algorithm to measure sea ice concentration with microwave radiometers, *J. Geophys. Res.*, *90*(C1), 1087–1099.

Vant, M. R., R. B. Gray, R. O. Ramseier, and V. Makios (1974), Dielectric properties of fresh and sea ice at 10 and 35 GHz, *J. Appl. Phys.*, *45*(11), 4712–4717.

Walsh, J. E., and C. M. Johnson (1979), An analysis of Arctic sea ice fluctuations, *J. Phys. Oceanogr.*, *9*, 580–591.

J. C. Comiso and C. L. Parkinson, Cryospheric Sciences Branch, NASA Goddard Space Flight Center, Code 614.1, Greenbelt, MD 20771, USA. (josefino.c.comiso@nasa.gov)